ACS Macro Letters

Viewpoint

pubs.acs.org/macroletters

Chirality Transfer in Block Copolymer Melts: Emerging Concepts

Gregory M. Grason*

Department of Polymer Science and Engineering, University of Massachusetts, Amherst, Massachusetts 01003, United States

ABSTRACT: Chirality transfer from molecule to assembly is a ubiquitous process, occurring in every class of self-assembling materials, from liquid crystals to biological matter. Yet, a basic understanding of the influence of molecular chirality on the mesoscopic assembly of block copolymers lags decades behind nearly all other aspects of their structure (e.g., chain composition, topology, stiffness, interactions). This Viewpoint highlights recent experimental and theoretical studies of mesochiral assemblies of chiral block copolymers that are beginning to shed light onto the necessary conditions for and principle outcomes of chirality transfer in block copolymer melts.

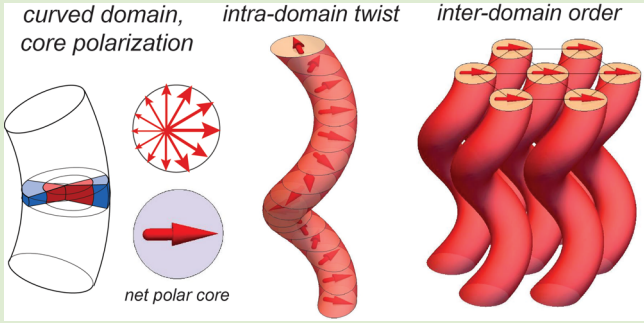

While block copolymers (BCPs) are well-known[1] and often exploited for their assembly into a rich spectrum of periodically ordered mesophases, the understanding how molecular chirality in one or more block influences the mirror symmetry (or lack thereof) of assembly at the mesoscale is only beginning to come into focus. Chirality transfer refers to the ability of a molecule to transmit its handedness, through the symmetry of its intermolecular packing, to the overall structure of assembly at a much larger, supramolecular length scale.[2] Beginning with Pasteur's famous discovery relating enantiomeric mm-scale habits of crystalline salts formed from right- or left-handed tartaric acid, chirality transfer has become a ubiquitous theme in molecular assembly,[3] documented in a broad range of systems: liquid crystals;[4,5] lipid membranes,[6,7] secondary/tertiary structure[8,9] and hierarchical ordering[10−14] of biomolecules (proteins and nucleic acids), supramolecular polymers and fibers,[15,16] and nanoparticles.[17,18] Indeed, Nature makes great use of chirality transfer from extracellular molecules like chitin[10] to mesoscale assemblies (∼10−100 nm) to guide the formation of a remarkable class of photonically active nanostructures that have been identified in recent studies of diverse living organisms, such as jeweled beetles[19] and iridescent butterflies.[20,21] Despite these broad implications of chirality transfer in self-assembly at large, the understanding of the influence of chain chirality on the otherwise well-known BCP phase diagram is still in its infancy. This Viewpoint highlights the recent convergence of experimental and theoretical research on assembly of chiral block copolymer (BCP*) melts and the emergence of new paradigms and questions regarding mechanisms of chirality transfer that underlie the stability of mesochiral morphologies observed and yet to be discovered.

Observations of Chirality Transfer in BCP*s: Chiral morphologies are observed in a range of polymer systems, both intrinsically chiral and achiral. In the bulk, examples include spontaneous chiral morphologies, which have equal probability to form right- or left-handed order, emerging from the assembly of achiral BCP melts, such as cylinder[22] and network[23] morphologies observed in terblock polymers, as well as helical phases predicted for rod−coil diblock assemblies.[24−26] In semicrystalline achiral polymers, helicoidally twisted lamella also form with spontaneously selected handedness,[27] whereas similar morphologies formed in chiral polymers have been shown to exhibit chirality transfer to helicoid handedness.[28−32] In solution assemblies, several groups have demonstrated the chirality transfer to isolated helical micelle morphologies of peptide-based copolymers.[33−35]

Despite the extensive study of the relationship between molecular structure and BCP melt thermodynamics in recent decades, the generic influence of intrinsic chirality at the monomer scale on the formation of periodically ordered BCP mesodomains is largely unknown. Experimental evidence for chirality transfer has emerged only recently in bulk BCP assemblies from studies of polylactic acid (PLA) based copolymers by Ho and co-workers.[36−39] The lactide monomer of PLA possesses two chiral centers, and polymerization of stereopure D or L lactide enantiomers yields chiral polymers PDLA or PLLA, respectively (Figure 1A,B). In a series of studies,[36,38−41] Ho and co-workers have studied the assembly of diblocks composed of PDLA or PLLA covalently linked to an achiral polystyrene (PS) block. In contrast to achiral diblocks which form the standard, mirror-symmetric phase of hexagonally packed and parallel cylinders (C), PS−PLLA or PS−PDLA diblocks assemble into hexagonally ordered arrays of homochiral helical domains, denoted as the H* phase, where the core of tubular domains is composed of the chiral blocks (Figure 1F). Notably, the dimensions associated with mesochiral order of the domain (helical pitch and radius, 140

Received: February 17, 2015
Accepted: April 15, 2015
Published: April 20, 2015

DOI: 10.1021/acsmacrolett.5b00131
ACS Macro Lett. 2015, 4, 526−532

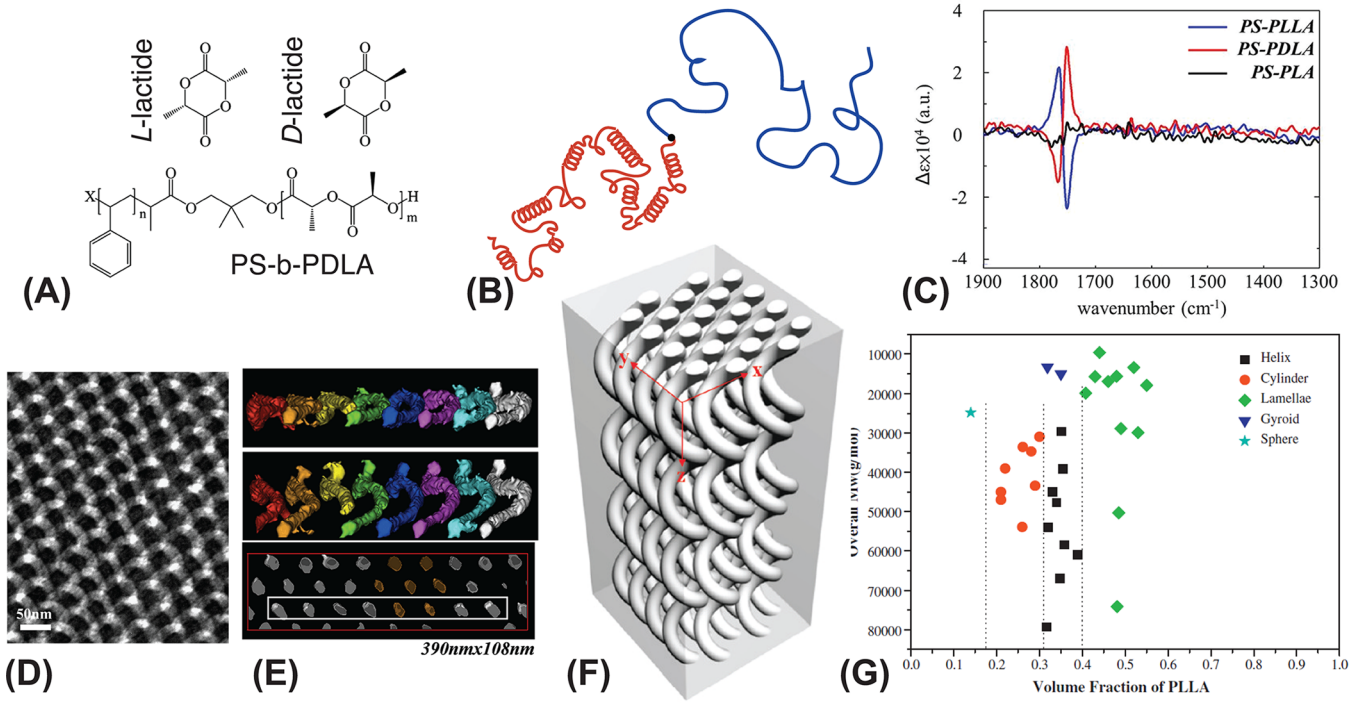

Figure 1. (A) Chemical structure of PS−PDLA, where the chiral PDLA block is synthesized by ring-opening of chiral D-lactide, which possesses two chiral carbons; (B) Cartoon of hypothesized transfer of monomer chirality to "helically-persistent" flexible conformations of P(D or L)LA block. (C) Spectra from VCD from films cast from PS−PLA showing opposite differential absorption from when PS−PLLA and PS−PDLA spectra respective and zero chiral signal from racemic PS−PLA. (D) TEM image of a section of H* morphology of PS−PLLA, whose 3D morphology is reconstructed via EM-tomography in (E). (E) Schematic of the hexagonal packing of minor domains (chiral P(D or L)LA block) in the H* phase, and a phase portrait of observed morphology reports for PS−PLLA by Ho and co-workers. (A, C, and E are adapted from ref 39. Copyright 2012 American Chemical Society. D, F, and G are adapted from ref 38. Copyright 2009 American Chemical Society.)

and 50 nm, respectively) are orders of magnitude larger than the chiral lactide monomer size.

Experimental studies of PS-P(D or L)LA assembly have shed important light onto several key aspects of the chirality transfer process from lactide monomer to H* mesophase. First, using TEM tomography (Figure 1E) to resolve 3D structure of helical domains,[39] the mesoscale handedness of the H* domains is shown to switch with a reversal of monomer chirality. Further, explorations of the PS−PLLA phase diagram[38] show further that chirality transfer exhibits a nontrivial dependence on the chiral composition, or length fraction f of the chiral block, including regions of both mesochiral (H*) and achiral (C) cylinder mesophases occurring at respectively, higher or lower windows of chiral composition (Figure 1G). Hence, even in a stereopure PS-P(D or L)LA possessing only L or D monomers, chirality transfer to the mesoscale is not automatic. Vibrational circular dichroism (VCD) studies of PS-P(D or L)LA solutions and bulk films suggest at least some measure of transfer of chirality to the helical conformations along the P(D or L)LA backbone (Figure 1C).[39] Helical backbone conformations are well-known for semicrystalline chiral polylactides,[42] however, as with C phase, packing considerations within the tubular core domain of H* phase are not compatible with the rod-like conformations implied by perfect helical intrachain structure. Indeed, time-resolved in situ scattering experiments,[43] casting PS-P(D or L)LA from a wide array of solvents, implies that crystalline ordering of the polylactide domain has an antagonistic relationship with the formation of H*. Under conditions where P(D or L)LA blocks rapidly crystallize, the H* is typically not formed, where as, when the microphase segregation proceeds rapidly relative to the P(D or L)LA crystallization rate, the H* morphology is observed with little or no detectable level of crystallinity.[44] Taken together, these results suggest that the H* phase is stabilized by an "amorphous" melt-like or more likely a weakly liquid-crystalline packing of P(D or L)LA blocks, which while globally coil-like must consist of local and transient sections of right- or left-hand helical conformations interrupted by sections of imperfect intrachain helical order (see Figure 1B).

Theory of BCP* Assembly: A common mechanism of chirality transfer in many self-assembling systems is the tendency to introduce "twisted" textures in molecular orientation.[45] For example, in chiral liquid crystals, the introduction of chiral groups on mesogens or chiral dopants into an achiral guest phase typically stabilizes the cholesteric texture characterized by a helical rotation of director throughout the sample. Notably, the pitch p of this rotation is mesoscopic ~100 nm to 10 μm, orders of magnitude larger than the molecular scale.[2] While the relationship between chiral molecular structure and ideal pitch is far from clear,[46] the effective degree of chirality, or the chiral strength, of a system is conveniently quantified by the inverse pitch, or $q_0 = 2\pi/p$, with strong chirality characterized by short pitches (or large $|q_0|$) stabilized by relatively larger intermolecular skews.

To understand mechanisms of mesochiral morphology formation in melt state BCP*s, Zhao et al. have recently developed an equilibrium model of BCP*s in which chirality enters as an intrinsic preference for cholesteric ordering of chiral block[47] (Figure 2). Hence, this model may apply chiral intersegment forces in the apparently melt-state packing of "helically persistent" chiral blocks of PS-P(D or L)LA, or

DOI: 10.1021/acsmacrolett.5b00131
ACS Macro Lett. 2015, 4, 526−532

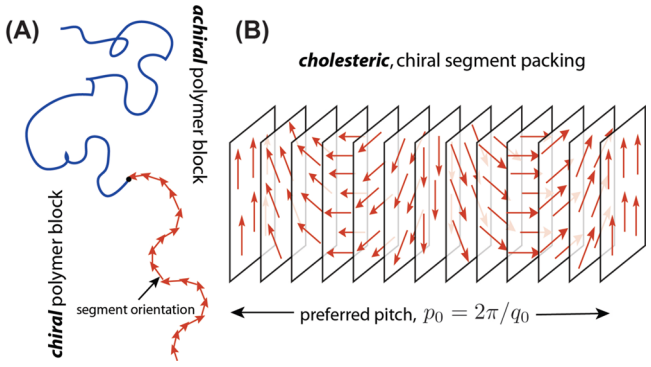

Figure 2. Schematic of oSCF model of BCP* melts studied by Zhao et al. (A) Average orientation of chiral block segments (A-block) is described by a spatially varying, self-consistent vector order parameter; (B) Schematic of the preferred cholesteric twist of the order parameter.

instead, to BCP*s possessing main chain, cholesteric forming mesogens. This approach determines the free energy of a melt configuration in terms of three contributions,

$$F = \rho_0 \int dV \chi \varphi_A(\mathbf{x})\varphi_B(\mathbf{x}) - S_{chain} + F^*$$

where the first term represents the mixing enthalpy of unlike segments (of volume ρ_0^{-1}) and the second contribution denotes the entropic cost to perturb polymer chains from random-walk (freely jointed chain) statistics. The third free energy term is unique to theory of chiral copolymers, representing the intrinsic preference for cholesteric twist of the orientation of chiral block segments (here, A-block segments),

$$F^*[\mathbf{t}(\mathbf{x})] = \frac{\rho_0}{2}\int dV[K_1(\nabla\cdot\mathbf{t})^2 + K_2(\nabla\times\mathbf{t})^2 + 2q_0K_2\mathbf{t}\cdot(\nabla\times\mathbf{t})]$$

Here, $\mathbf{t}(\mathbf{x})$ is a vector order parameter corresponding to the local average of $\hat{\mathbf{t}}_\alpha$, the polar orientation of the αth A-block segment in the melt, $\mathbf{t}(\mathbf{x}) = \rho_0^{-1}\sum_{\alpha\in A}\hat{\mathbf{t}}_\alpha\delta(\mathbf{x}-\mathbf{x}_\alpha)$ and K_1 and K_2 are Frank elastic constants. The presence of chirality at the segment scale corresponds to the case $q_0 \neq 0$, and a thermodynamic preference for a nonzero cholesteric twist of segments, $\mathbf{t}\times(\nabla\times\mathbf{t}) \neq 0$.[2] The minimal free energy configuration of $\mathbf{t}(\mathbf{x})$ is a cholesteric texture with pitch $p = 2\pi/q_0$; hence, the magnitude of q_0 serves a phenomenological measure of the segment scale chiral strength (see Figure 2). Like the χ parameter that describes at a coarse-grained level scalar interactions between segments, the Frank constants and q_0 itself derive from orientation-dependent interactions between chiral segments (see, e.g., ref 48). At present, no systematic study has been conducted theoretically or computationally to quantify these parameters for a realistic molecular model of an "amorphous" and flexible chiral polymer. Nonetheless, one can estimate entropic contributions to these constants based on the Onsager picture of steric interactions between rod-like sections of length a and density ρ_0,[49] suggesting (in units of k_BT) that $K_i \sim \rho_0 a^5$. In addition to a first-principles prediction from atomistic structure of chiral polymer backbones, a likely more viable and accurate approach will be to quantify these coarse-grained orientational free-energy parameters from experimental measurements, much like the quantification of the χ parameter. For example, the preferred pitch could be observed for pure chiral homopolymer that exhibits a chiral mesomorphic behavior, and a series of

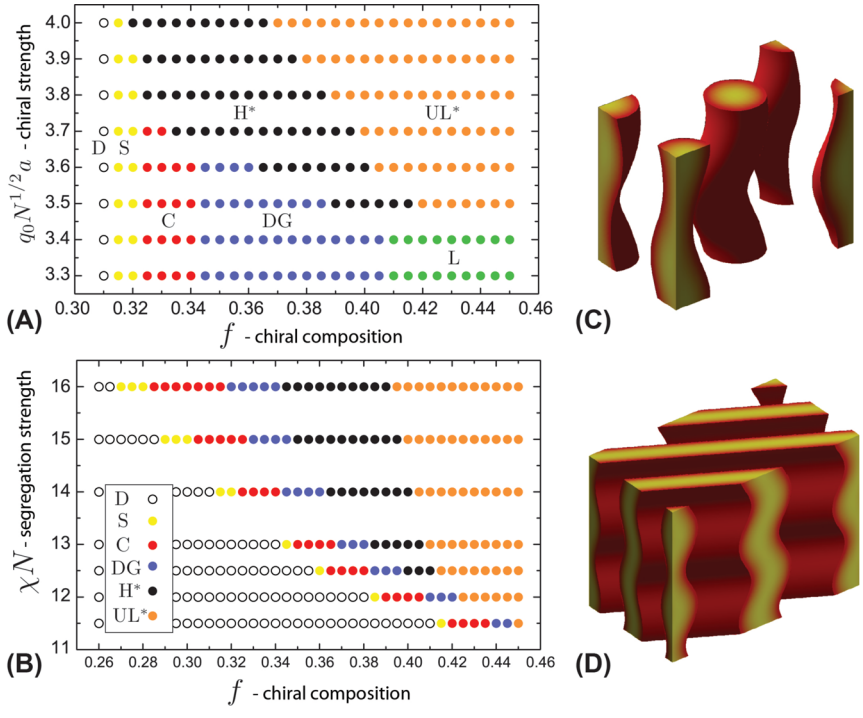

Figure 3. Minority chiral component and weak segregation oSCF phase diagrams:[47] (A) fixed segregation ($\chi N = 14$); (B) fixed chiral strength ($\overline{q} = 3.6$). Along with standard achiral morphologies (L, lamella; C, cylinder; S, sphere; DG, double-gyroid), chirality stabilizes two new morphologies: H*, helical cylinder, and UL*, undulated lamella (whose chiral block composition profiles are shown in C and D, respectively). Figures adapted with permission from ref 47. Copyright 2013 American Physical Society.

DOI: 10.1021/acsmacrolett.5b00131
ACS Macro Lett. 2015, 4, 526−532

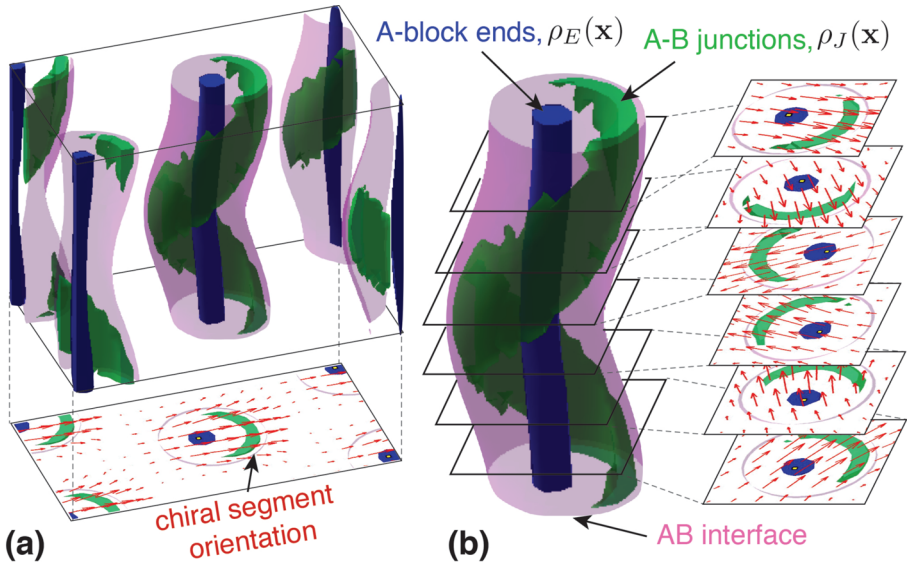

Figure 4. oSCF solution of equilibrium H* morphology of BCP* melts (figure based on work of ref 56). The AB interface ($\phi_A = \phi_B = 0.5$ contour) is shown as transparent purple surface, and blue and green surfaces shown high-density contours of (chiral) A-block ends and A-B junction points. In horizontal sections, profiles of mean chiral segment orientation, $\mathbf{t}(\mathbf{x})$, are indicated by red arrows. A unit cell of H* is shown in A, while B highlights the rotation of the domain and cholesteric twist of segments along the backbone of the helical domain.

standard experimental methods could be applied to extract Frank constants from the mesomorphic phase of a given chiral homopolymer.[50]

An "orientational self-consistent field" (oSCF) theory[48] describes the mean-field relationship between chain configurations, A and B composition profiles $\phi_A(\mathbf{x})$ and $\phi_B(\mathbf{x})$ and mean orientation of chiral segments $\mathbf{t}(\mathbf{x})$, which is solved to predict equilibrium BCP* morphologies and their corresponding free energies. In addition to the parameters χN and A-composition f standard to the density-dependent SCF theory,[51] the vector oSCF theory of chiral BCP melts introduces parameters describing the cost of distortions from the ideal segment twist, which are made dimensionless by comparison to the mean-square size of chain in the disordered state: scaled Frank constants $\overline{K}_i = K_i/Na^2$ and scaled chiral strength $\overline{q} = q_0 N^{1/2} a$ (with segment size a). These parameters define the thermodynamic axes controlling chirality transfer in the BCP* phase diagram. A similar model was employed in a recent classical density-functional field theory study of BCP* assembly,[52] yielding at least qualitatively similar morphologies, though phase behavior was not addressed in this study.

At present, the vast parameter space of BCP* melts and the computational burden of solving oSCF equations for segment distributions[48] in 3D geometries have limited calculations to weakly segregated ($\chi N < 16$) and minority chiral composition ($f < 0.5$) melts.[47] Figure 3A,B shows oSCF phase diagrams of single-block chiral diblock melts calculated in terms of three parameters (fixing $\overline{K}_1 = \overline{K}_2 = 1/2$): chiral composition, f; reduced chiral strength, $\overline{q}$; and segregation strength, χN. Despite the narrow parameter range, this study reveals two critical aspects of chirality transfer in BCP melts:

(i) Chirality transfer from segments to mesophase is a nonlinear function of chiral strength and composition: As shown in Figure 3A, at fixed segregation strength, we predict a critical segment chirality $\overline{q}_c = 3.45$, below which the self-assembled mesophases retain the mirror or inversion symmetric structures of achiral copolymers. Above this critical measure of chirality, two equilibrium morphologies are stabilized by the cholesteric twisting of segments in the chiral domains: the H* phase of hexagonally ordered helical columns (Figure 3C) and a new undulated lamellar morphology, dubbed the UL* phase (Figure 3D). Hence, oSCF theory confirms that the H* morphology is indeed an equilibrium phase of BCP* melts. Further, it confirms that chirality transfer in the cylinder morphologies is not automatic: for fixed χN and large chirality ($\overline{q} > \overline{q}_c$) both achiral C and chiral H* phase are stable in distinct composition windows. The apparent threshold nature of chirality transfer to morphology may account, in part, for the current lack of observed mesochiral morphologies beyond polylactide-based BCP*s, despite the wide chemistries available for chiral polymer blocks (say, e.g., enantiomeric polypropylenes). Notably, the H* morphology has also recently been reported for achiral BCPs doped with low-molecular-weight chiral additives (D- or L-tartaric acid), which presumably drive intersegment twist in the H-bond accepting achiral block.[53]

(ii) Chirality transfer in cylindrical BCP morphologies occurs via a thermodynamic coupling between domain shape and segment orientation: The predicted segment orientation within the mesochiral H* phase reveals a twisted, cholesteric segment texture is threaded within the chiral core of the domain with the pitch axis along the pitch of the helix (Figure 4), while a similar underlying cholesteric pattern underlies the rippling the UL* phase.[54] Previous experiments to probe the nature of chiral chain packing by Ho and co-workers[39] have exploited the orientation dependence of VCD spectral features deriving from intermolecular coupling between planar, dye groups placed at the interblock junction of PS−PLLA diblocks. Spectral VCD shifts from H* phase of PS−PLLA relative to C phase of PS−PLA, indicate some measure of local rotation between the axes of dyes, and presumably, also the diblock backbone at the interface consistent with the patterns of cholesteric twist predicted by the oSCF theory.

Open Questions: Notwithstanding the encouraging qualitative agreement between oSCF theory and PS-P(D or L)LA experiments regarding the formation of the H* phase, numerous challenges to understanding chirality transfer in

DOI: 10.1021/acsmacrolett.5b00131
ACS Macro Lett. 2015, 4, 526−532

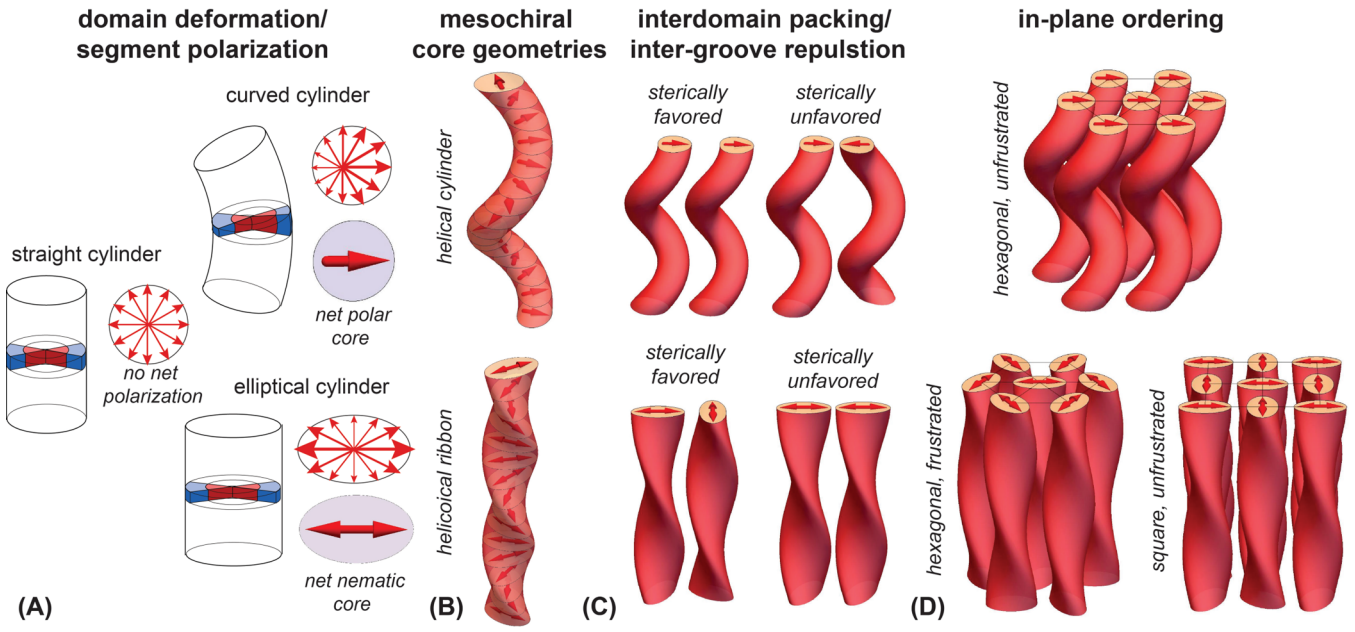

Figure 5. Heuristic model of multiscale mesochiral ordering columnar BCP* phases. (A) Depictions of columnar domains possessing the straight cylindrical geometry of the C phase as well as the curved backbone of H* and a elliptical "warping" of cross-section are shown, along with corresponding "wedges" highlighting the single-chain volume distributions and the corresponding distributions of chiral block orientations. The latter highlight the lack of net polarization of chiral blocks in isotropic cylinders, while curved and elliptic cylinders lead to net polar and "nematic" ordering core blocks, respectively. The twisted stacking of curved cylinder and elliptical cylinder sections leads to mesochiral columnar morphologies, helical cylinders, and helicoidal ribbons, respectively (B). The geometry of favorable and unfavorable packing of neighbor domains is shown in (C). Conjectured candidates for optimal lateral packing of helical cylinder (H*) and helicoidal ribbon (HR*) morphologies are shown in (D).

BCP* melts remain. Foremost among these remains the need experimentally quantify the coarse-grained chiral parameters, q_0 and K_i, so as to place specific chemistries onto BCP* phase diagrams and to enable the extension of chirality transfer to new chiral chemistries. Second, while VCD experiments of dye-labeled copolymers indicate some measure of twist to the AB interface,[39] it remains an experimental challenge to directly resolve the spatial patterns of chiral segment twist throughout the complex 3D geometry of chiral domains. Finally, beyond the experimentally observed and theoretically predicted H* phases, possible mechanisms of chirality transfer to other morphologies (e.g., spheres, networks, etc.) remain to be understood.

We conclude with a brief overview of the heuristic model describing the coupling between mesochiral domain shape and cholesteric intradomain twist for columnar mesophases (Figure 5), which illustrates the broader possibilities of for as yet undiscovered mesochiral symmetries in the BCP* phase diagram. As argued in ref 47, threading cholesteric order within core domains of columnar structures requires a disruption of the net isotropic packing of minor blocks in the C phase: a simple "twisted" stacking of these isotropic sections leads to no net cholesteric twist, as measured by the spatial average of $\mathbf{t} \cdot (\nabla \times \mathbf{t})$. For bent domains like H*, packing constraints and domain curvature lead to an asymmetry in chain stretching around the core domain (in accordance with the local curvature distribution of the AB interface), and further imply a net polarization in chiral block segments proportional to the degree of domain bending (Figure 5A). Twisted stacking of such "polarized" sections, therefore, results in a net cholesteric, intradomain twist and the helical rotation of bending direction along domain (Figure 5B).

An alternative mode of introducing intradomain twist is depicted in Figure 5A,B, where cross sections of columnar BCP domains are locally deformed elliptically. The distribution of curvature around these anisotropic sections implies larger (smaller) chain stretching along the major (minor) axes and a result in a net "nematic" ordering of segments in sections along the major axis. A twisted stacking of these anisotropic sections around a straight centerline therefore threads a net cholesteric order through the domain, resulting in a "helicoidal ribbon" morphology, which we might refer to as HR* (Figure 5B). Similar, spontaneously chiral helicoidal morphologies have been predicted for simulations of rod−coil BCPs;[24,26] however, to date, such a HR* morphology has not been observed experimentally nor predicted in the oSCF theory for chiral diblocks.

The current absence of an observed HR* phase may ultimately derive from a large cost (interfacial and chain stretching) relative to the gain in intradomain cholesteric ordering, though it is illuminating to consider generic costs of interdomain packing which may further tip the balance between HR* and H* phases. Entropic preferences to maximize interdomain volume available for matrix chains corresponds effectively repulsive interactions between neighbor "grooves" of mesochiral domains (Figure 5C). For H*, which possesses a single-helical symmetry, optimal packing corresponds to "alignment" between neighbor domain polarization, whereas, for HR* with its double-helical symmetry, aligned domain directors correspond to maximally unfavorable groove contact and optimal packing (interlocked grooves) corresponds to perpendicular directors. While the 6-fold symmetry of hexagonal packing presents no obstacles to aligned domain polarization of neighbors in H*, "anti-nematic" domain interactions of the type described for HR* are naturally

DOI: 10.1021/acsmacrolett.5b00131
ACS Macro Lett. 2015, 4, 526−532

frustrated on hexagonal lattices due to the impossibility of perpendicular alignment of all nearest neighbors. Double-helical packing models (commonly studied for ordered DNA phases)[54,55] predict two possible results of this type of lattice frustration (shown in Figure 5D). In one case, hexagonal symmetry remains but neighbor domains remain at a maximum interdomain tilt of 60° due to the lattice frustration; in the second case, the 6-fold lattice symmetry is broken (by, for example, adopting the square lattice), allowing perpendicular domain alignment between all neighbors. While the thermodynamically optimal order for a putative HR* phase of BCP*s is not obvious, it is clear that the excess cost of interdomain frustration between double-helical columns will tend to bias the formation of H* whose interdomain packing is unfrustrated (Figure 5D).

A rigorous analysis of the thermodynamic competition between "polar" and "nematic" mesochiral columnar ordering in BCP* melts remains to be explored. Beyond columnar morphologies, it is further quite possible that the optimal symmetry of intradomain twist varies with BCP* morphologies (e.g., networks, spheres, columns), leading to a host of yet unimagined mesochiral structures to be explored in the largely uncharted BCP* phase diagram.

AUTHOR INFORMATION

Corresponding Author

*E-mail: grason@mail.pse.umass.edu.

Notes

The authors declare no competing financial interest.

ACKNOWLEDGMENTS

Related work in the author's research group has been supported by the NSF through the UMass MRSEC DMR-0820506 and the Center for Hierarchical Manufacturing CMMI-10250220. The author would like to acknowledge W. Zhao, I. Prasad, E. Thomas, and R.-M. Ho for comments and discussions useful in the preparation of this manuscript.

REFERENCES

(1) Bates, F. S.; Fredrickson, G. H. *Annu. Rev. Phys. Chem.* **1990**, *41*, 525−557.
(2) Harris, A.; Kamien, R.; Lubensky, T. *Rev. Mod. Phys.* **1999**, *71*, 1745−1757.
(3) Wang, Y.; Xu, J.; Wang, Y.; Chen, H. *Chem. Soc. Rev.* **2013**, *42*, 2930−2962.
(4) Goodby, J. W. *J. Mater. Chem.* **1991**, *1*, 307.
(5) Chilaya, G. *Mol. Cryst. Liq. Cryst.* **2012**, *561*, 8−35.
(6) Spector, M. S.; Selinger, J. V.; Schnur, J. M. Chiral Molecular Assembly. In *Materials−Chirality*; Green, M. M.; Nolte, R. J. M.; Meijer, E. W., Eds.; Wiley: New York, 2003; Vol. *24*.
(7) Selinger, J. V.; Spector, M. S.; Schnur, J. M. *J. Phys. Chem. B* **2001**, *105*, 7157−7169.
(8) Crick, F. H. C. *Acta Crystallogr.* **1953**, *6*, 689−697.
(9) Parry, D. A. D.; Fraser, R. D. B.; Squire, J. M. *J. Struct. Biol.* **2008**, *163*, 258−269.
(10) Neville, A. C. *Biology of Fibrous Composites: Development Beyond the Cell Membrane*; Cambridge University Press: Cambridge, 1993.
(11) Bouligand, Y. *Comptes Rendus Chim.* **2008**, *11*, 281−296.
(12) Livolant, F.; Leforestier, A. *Prog. Polym. Sci.* **1996**, *21*, 1115−1164.
(13) Aggeli, A.; Nyrkova, I. A.; Bell, M.; Harding, R.; Carrick, L.; McLeish, T. C.; Semenov, A. N.; Boden, N. *Proc. Natl. Acad. Sci. U.S.A.* **2001**, *98*, 11857−11862.
(14) Grason, G. M.; Bruinsma, R. F. *Phys. Rev. Lett.* **2007**, *99*, 098101.
(15) Brunsveld, L.; Folmer, B. J. B.; Meijer, E. W.; Sijbesma, R. P. *Chem. Rev.* **2001**, *101*, 4071−4097.
(16) Brizard, A.; Oda, R.; Huc, I. *Top. Curr. Chem.* **2005**, *256*, 167−218.
(17) Jadzinsky, P. D.; Calero, G.; Ackerson, C. J.; Bushnell, D. A.; Kornberg, R. D. *Science* **2007**, *318*, 430−433.
(18) Gautier, C.; Bürgi, T. *ChemPhysChem* **2009**, *10*, 483−492.
(19) Sharma, V.; Crne, M.; Park, J. O.; Srinivasarao, M. *Science* **2009**, *325*, 449−451.
(20) Michielsen, K.; Stavenga, D. G. *J. R. Soc. Interface* **2008**, *5*, 85−94.
(21) Saranathan, V.; Osuji, C. O.; Mochrie, S. G. J.; Noh, H.; Narayanan, S.; Sandy, A.; Dufresne, E. R.; Prum, R. O. *Proc. Natl. Acad. Sci. U.S.A.* **2010**, *107*, 11676−11681.
(22) Krappe, U.; Stadler, R.; Voigt-Martin, I. *Macromolecules* **1995**, *28*, 4558−4561.
(23) Epps, T. H.; Cochran, E. W.; Bailey, T. S.; Waletzko, R. S.; Hardy, C. M.; Bates, F. S. *Macromolecules* **2004**, *37*, 8325−8341.
(24) Horsch, M. A.; Zhang, Z.; Glotzer, S. C. Self-Assembly of Polymer-Tethered Nanorods. *Phys. Rev. Lett.* **2005**, *95*.
(25) Kriksin, Y. A.; Khalatur, P. G. *Macromol. Theory Simulations* **2012**, *21*, 382−399.
(26) Kriksin, Y. a.; Tung, S.-H.; Khalatur, P. G.; Khokhlov, a. R. *Polym. Sci., Ser. C* **2013**, *55*, 74−85.
(27) Keith, H. D.; Padden, F. J. *Polymer* **1984**, *25*, 28−42.
(28) Li, C.; Cheng, S.; Ge, J.; Bai, F.; Zhang, J.; Mann, I.; Harris, F.; Chien, L.-C.; Yan, D.; He, T.; et al. *Phys. Rev. Lett.* **1999**, *83*, 4558−4561.
(29) Li, C. Y.; Cheng, S. Z. D.; Ge, J. J.; Bai, F.; Zhang, J. Z.; Mann, I. K.; Chien, L.-C.; Harris, F. W.; Lotz, B. *J. Am. Chem. Soc.* **2000**, *122*, 72−79.
(30) Wang, J.; Li, C. Y.; Jin, S.; Weng, X.; Van Horn, R. M.; Graham, M. J.; Zhang, W.-B.; Jeong, K.-U.; Harris, F. W.; Lotz, B.; et al. *Ind. Eng. Chem. Res.* **2010**, *49*, 11936−11947.
(31) Maillard, D.; Prud'homme, R. E. *Macromolecules* **2006**, *39*, 4272−4275.
(32) Maillard, D.; Prud'homme, R. E. *Macromolecules* **2008**, *41*, 1705−1712.
(33) Zhong, S.; Cui, H.; Chen, Z.; Wooley, K. L.; Pochan, D. J. *Soft Matter* **2008**, *4*, 90.
(34) Murnen, H. K.; Rosales, A. M.; Jaworski, J. N.; Segalman, R. A.; Zuckermann, R. N. *J. Am. Chem. Soc.* **2010**, *132*, 16112−16119.
(35) Wang, J.; Lu, H.; Kamat, R.; Pingali, S. V.; Urban, V. S.; Cheng, J.; Lin, Y. *J. Am. Chem. Soc.* **2011**, *133*, 12906−12909.
(36) Ho, R. M.; Chiang, Y. W.; Tsai, C. C.; Lin, C. C.; Ko, B. T.; Huang, B. H. *J. Am. Chem. Soc.* **2004**, *126*, 2704−2705.
(37) Ho, R.-M.; Chen, C.-K.; Chiang, Y.-W. *Macromol. Rapid Commun.* **2009**, *30*, 1439−1456.
(38) Ho, R. M.; Chiang, Y. W.; Chen, C. K.; Wang, H. W.; Hasegawa, H.; Akasaka, S.; Thomas, E. L.; Burger, C.; Hsiao, B. S. *J. Am. Chem. Soc.* **2009**, *131*, 18533−18542.
(39) Ho, R.-M.; Li, M.-C.; Lin, S.-C.; Wang, H.-F.; Lee, Y.-D.; Hasegawa, H.; Thomas, E. L. *J. Am. Chem. Soc.* **2012**, *134*, 10974−10986.
(40) Chiang, Y.-W.; Ho, R.-M.; Ko, B.-T.; Lin, C.-C. *Angew. Chem., Int. Ed.* **2005**, *44*, 7969−7972.
(41) Ho, R. M.; Chiang, Y. W.; Lin, S. C.; Chen, C. K. *Prog. Polym. Sci.* **2011**, *36*, 376−453.
(42) Garlotta, D. *J. Polym. Environ.* **2001**, *9*, 63−84.
(43) Zhao, W.; Liu, F.; Wei, X.; Chen, D.; Grason, G. M.; Russell, T. P. *Macromolecules* **2013**, *46*, 474−483.
(44) Zhao, W.; Chen, D.; Grason, G. M.; Russell, T. P. *Macromolecules* **2013**, *46*, 455−462.
(45) De Gennes, P. G.; Prost, J. *The Physics of Liquid Crystals*, 2nd ed.; Oxford University Press: Oxford, 2007.
(46) Harris, a.; Kamien, R.; Lubensky, T. *Phys. Rev. Lett.* **1997**, *78*, 1476−1479.
(47) Zhao, W.; Russell, T.; Grason, G. *Phys. Rev. Lett.* **2013**, *110*, 058301.

DOI: 10.1021/acsmacrolett.5b00131
ACS Macro Lett. 2015, 4, 526−532

(48) Zhao, W.; Russell, T. P.; Grason, G. M. *J. Chem. Phys.* **2012**, *137*, 104911.
(49) Straley, J. P. *Phys. Rev. A* **1976**, *14*, 1835−1841.
(50) DuPré, D. B.; Duke, R. W.; Dupre, D. B. *J. Chem. Phys.* **1975**, *63*, 143.
(51) Matsen, M. W. *J. Phys.: Condens. Matter* **2001**, *14*, R21−R47.
(52) Wang, S.; Kawakatsu, T.; Chen, P.; Lu, C. D. *J. Chem. Phys.* **2013**, *138*, 194901.
(53) Yao, L.; Lu, X.; Chen, S.; Watkins, J. J. *Macromolecules* **2014**, *47*, 6547−6553.
(54) While the A/B composition profile of the undulated lamellar phase is mirror symmetric, the morphology is chiral due to the underlying pattern of (cholesteric) chain orientation.
(55) Grason, G. M. *Europhys. Lett.* **2008**, *83*, 7.
(56) Zhao, W. *Helical Ordering in Chiral Block Copolymers*; University of Massachussetts: Amherst, 2012.

DOI: 10.1021/acsmacrolett.5b00131
ACS Macro Lett. 2015, 4, 526−532